Journal of Hepatocellular Carcinoma

Dovepress
Taylor & Francis Group

Open Access Full Text Article

ORIGINAL RESEARCH

Single-Cell RNA Sequencing Integrated with Bulk-RNA Sequencing Analysis Reveals Prognostic Signatures Based on PANoptosis in Hepatocellular Carcinoma

Jiyin Wang[1–5,*], Xue Yin[1–4,6,*], Ziyi Li[1–4,*], Pu Liang[1–4,*], Yipeng Wang[1–4], Xingling Li[1–4], Wenying Qiao[1–4], Chaoyang Xiong[1–4], Minghang Yu[1–4], Xiaoyan Ding[1–4], Xi Wang[1–4,7]

[1]National Key Laboratory of Intelligent Tracking and Forecasting for Infectious Diseases, Beijing Ditan Hospital, Capital Medical University, Beijing, People's Republic of China; [2]Beijing Key Laboratory of Viral Infectious Disease, Institute of Infectious Diseases, Beijing Ditan Hospital, Capital Medical University, Beijing, People's Republic of China; [3]Beijing Institute of Infectious Diseases, Beijing, People's Republic of China; [4]National Center for Infectious Diseases, Beijing Ditan Hospital, Capital Medical University, Beijing, People's Republic of China; [5]HBV Infection, Clinical Cure and Immunology Joint Laboratory for Clinical Medicine, Capital Medical University, Beijing, People's Republic of China; [6]Department of Infectious Disease, The Third Xiangya Hospital, Central South University, Changsha, Hunan, 410013, People's Republic of China; [7]Department of Oncology, Capital Medical University, Beijing, People's Republic of China

*These authors contributed equally to this work

Correspondence: Xiaoyan Ding; Xi Wang, National Key Laboratory of Intelligent Tracking and Forecasting for Infectious Diseases, Beijing Ditan Hospital, Capital Medical University, Beijing, People's Republic of China, Tel/Fax +86-13811560276; +86-17316198975, Email dingxiaoyan198111@163.com; xiwang@ccmu.edu.cn

Purpose: Drug resistance severely compromises therapeutic efficacy in hepatocellular carcinoma (HCC); however, the selection of precise treatment strategies for patients remains a critical unmet clinical need. This study investigated PANoptosis-related mechanisms underlying HCC progression to identify actionable therapeutic targets and optimize patient-specific treatment outcomes.

Patients and Methods: Multi-omics analysis (single-cell/bulk RNA sequencing) combined with machine learning was used to identify the PANoptosis-related prognostic features. The association of PANoptosis-related expression with the tumor immune microenvironment and drugs was explored using bioinformatic analysis and experimental studies.

Results: High PANoptosis risk exhibited immunosuppressive microenvironments and therapeutic resistance. The PANoptosis-related gene YIF1B has emerged as a dual prognostic biomarker and tumor driver that promotes proliferation, and is linked to immune dysfunction and drug resistance.

Conclusion: YIF1B may be a promising therapeutic target. This PANoptosis framework bridges molecular mechanisms to clinical management, offering strategies for personalized HCC therapy and overcoming treatment resistance.

Keywords: PANoptosis, hepatocellular carcinoma, YIF1B, drug resistant

Introduction

The predominant late-stage detection pattern of hepatocellular carcinoma (HCC), which accounts for the third highest global cancer mortality burden, significantly diminishes the clinical value of potentially curative surgical procedures.[1,2] Although hepatectomy demonstrates therapeutic efficacy, over half of the patients experience frequent postsurgical recurrence.[3,4] Current first-line therapy for unresectable HCC combines tyrosine kinase inhibitors (TKIs) with PD-1 blockade, achieving improved clinical responses compared to monotherapy.[5,6] However, durable responses remain limited by primary resistance in 20–30% of patients and eventual acquired resistance in responders.[7,10] These challenges underscore the urgent need for robust molecular biomarkers to enable early detection, predict therapeutic responses, and guide precise treatment strategies for this aggressive malignancy.

Received: 27 April 2025
Accepted: 23 July 2025
Published: 29 July 2025

Graphical Abstract

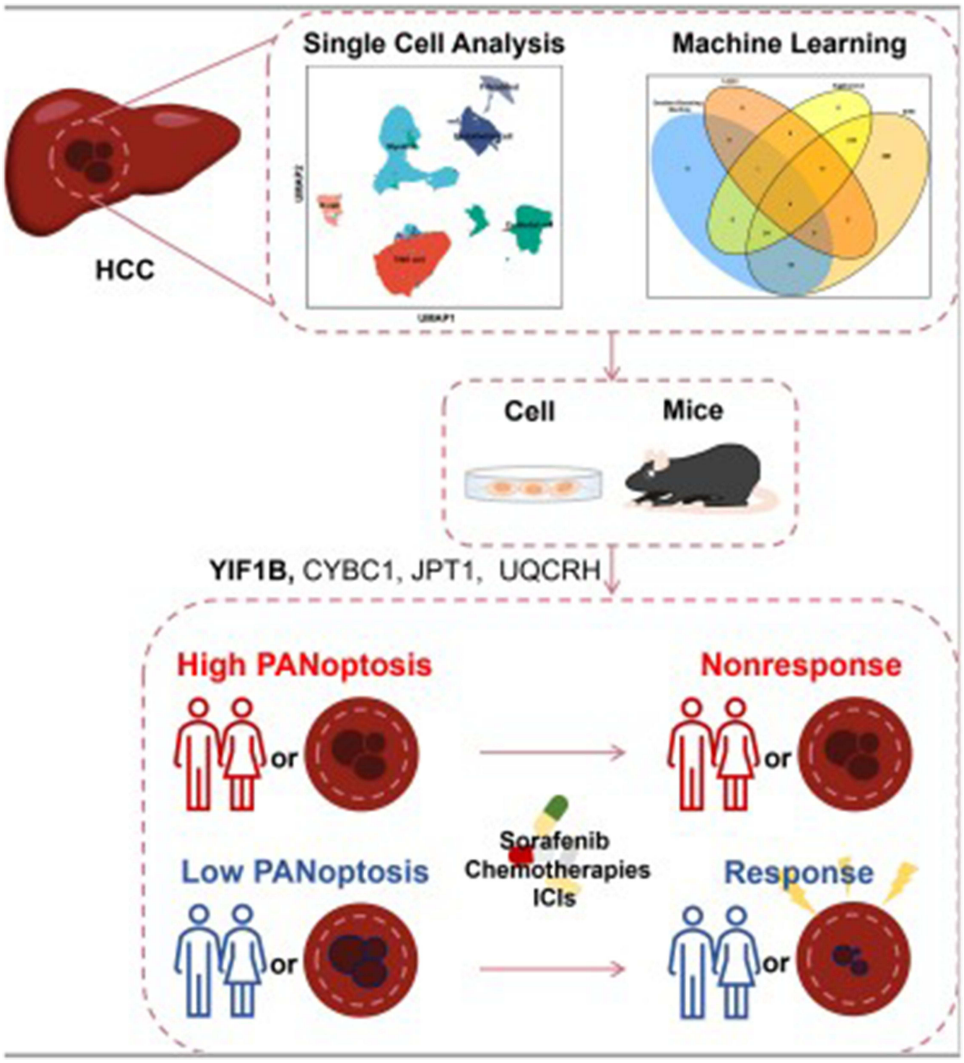

The pathogenesis of HCC involves complex immune interactions, particularly alterations in immune cell components, HCC-specific immune microenvironments, and evasion of programmed cell death (PCD).[11] As a pivotal modulator of tumor immunosuppression, PCD dysregulation promotes both tumorigenesis and therapeutic resistance.[12] Three classical PCD pathways, pyroptosis, apoptosis, and necroptosis exhibit extensive crosstalk, culminating in the recently identified inflammatory PCD modality termed PANoptosis.[13,15] Distinct from the isolated activation of individual pathways, PANoptosis integrates the features of all three forms through Z-DNA-binding protein 1 (ZBP1)-mediated PANoptosome complex formation, demonstrating activation across multiple pathologies.[16,17] This coordinated cell death mechanism maintains tissue homeostasis by eliminating compromised cells, activating antitumor immunity, and overcoming drug resistance.[18,19] In HCC, elevated PANoptosis-related gene expression correlates with enhanced immunotherapy responsiveness and the enrichment of pathways involving DNA repair, drug metabolism, and immune receptor signaling.[20] A systematic investigation of PANoptosis in HCC may reveal novel pathogenic mechanisms and therapeutic targets, particularly in treatment-resistant cases.

This study employed an innovative integration of single-cell and bulk RNA sequencing to delineate the PANoptosis-related mechanisms in HCC. Using advanced machine learning algorithms, we identified key PANoptosis-related genes and developed a quantitative predictive framework, which validated for effective patient stratification and survival prediction. Comprehensive

analyses revealed significant associations between risk score and tumor immune infiltration patterns, microenvironment characteristics, and therapeutic sensitivity profiles. Notably, the PANoptosis-associated gene YIF1B has emerged as a critical driver of HCC, with functional validation demonstrating its tumor-promoting effects on proliferation and oncogenesis. These findings not only elucidate PANoptosis-mediated regulatory networks in HCC progression but also establish YIF1B emerges as a theranostic biomarker capable of prognostic stratification and therapeutic vulnerability identification.

Materials and Methods

Single Cell Sequencing Data Download and Processing

Single-cell RNA sequencing data from 11 HCC samples including 7 tumor tissues and 4 adjacent non-tumor tissue samples, were acquired from the GEO database (GSE202642). Using Seurat v4.3.0, raw data underwent quality control by filtering cells with mitochondrial gene content >10% or detected genes <200/>7000, retaining 84,609 high-quality cells. Post-normalization, we performed dataset integration, identified highly variable genes (HVGs), and conducted principal component analysis (PCA). Cell populations were annotated via SingleR v1.99.2 with canonical markers, followed by PANoptosis-associated gene quantification using the PercentageFeatureSet algorithm.

Transcriptome Data Download and Processing

HCC transcriptomic profiles were acquired from TCGA (*n*=332; TCGAbiolinks R package) and GSE16747 (*n*=98), excluding intrahepatic cholangiocarcinoma cases. All FPKM (fragments per kilobase per million mapped reads) data underwent log2-transformation for downstream analyses.

Acquisition of PANoptosis-Related Genes

PANoptosis-associated genes were identified from GeneCards (relevance score >1.0 threshold) for downstream analysis.

Calculation of PANoptosis Score and Selection of PANoptosis-Related Genes

We implemented a dual computational strategy to delineate PANoptosis-associated molecular networks in the TCGA-HCC cohort. ssGSEA, using the GSVA package, quantified the pathway enrichment scores for PANoptosis-related genes across samples. Concurrently, WGCNA identified co-expressed gene modules correlated with PANoptosis activity using optimized parameters (soft threshold=9, minModuleSize=4, deepSplit=4), merging highly similar modules (correlation<0.25), and assigning unclustered genes to grey modules. Module-trait correlation analysis revealed three PANoptosis-associated gene clusters, from which hub genes were extracted for functional validation.

Development and Validation of a PANoptosis-Driven Prognostic Signature

Four machine learning approaches (LASSO, SVM, GBM, XGBoost) screened PANoptosis-related biomarkers, with intersection analysis identifying four consensus genes (CYBC1, JPT1, UQCRH, YIF1B) for risk score construction. TCGA-HCC patients stratified by median risk score showed significant survival differences, with the model achieving time-dependent AUCs for 1/3/5-year survival, validated in GSE16747.

Correlation Analysis of Immune Infiltration and Mutation

ssGSEA demonstrated significant depletion of cytotoxic lymphocytes (CD8+ T/NK cells) in high-risk HCC, coupled with elevated immune evasion (TIDE/MSI) and diminished immunotherapy response. Somatic mutation profiles and copy number variations (CNV) of prognostic genes were analyzed in TCGA cohorts using mafTools. Waterfall plots contrasted risk groups, highlighting top 30 mutated genes. Tumor mutational burden (TMB) showed sex-specific stratification patterns across risk strata.

Drug Susceptibility Prediction

The drug half-maximal inhibitor concentration analysis of sorafenib and several chemotherapeutic and targeted agents for the high- and low-risk groups was conducted using the "pRRophetic" R package in HCC.

The Construction of a Nomogram

Multivariate Cox regression validated the PANoptosis risk score as an independent prognostic factor, outperforming conventional parameters. A composite nomogram integrating risk scores with clinicopathological features demonstrated superior predictive accuracy through a temporal ROC analysis. Decision curve analysis revealed an enhanced net clinical benefit compared with standard prognostic strategies, validating its utility for individualized risk stratification.

Cell Culture, Transfection, and Lentivirus Infection

HepG2 and Huh7 cells (National Institute of Biological Products, China) were maintained in DMEM with 10% FBS and 1% penicillin/streptomycin (Gibco) under standard conditions (37°C, 5% CO_2). Lentiviral-mediated YIF1B knockdown (shRNA sequences: CCATCACCAAGCTCAAGT, CCTTCTTGGGCTACAAA) and overexpression (pLVX-IRES-puro-YIF1B) were achieved using Lipofectamine 3000. Stable polyclonal populations were selected via 2-week puromycin treatment and validated for knockdown efficiency.

Western Blot

Protein lysates were prepared using RIPA-150 buffer with protease inhibitors. After SDS-PAGE separation (40 μg) and nitrocellulose transfer, membranes were probed overnight with primary antibodies: anti-GAPDH (Proteintech, 10494-1-AP) and anti-YIF1B (Abcam, ab188127), followed by species-matched secondary antibody incubation.

CCK-8 Cell Proliferation Assay

Cells were seeded into 96-well plates at a density of 1×10^3 cells per well. 10 μL CCK-8 was added to each well and incubated at 37 °C for 2 h. The cell proliferation ability was measured by the intensity of absorbance at 450 nm.

Cell Migration Assay

Transwell migration assays were performed using 24-well cell culture inserts with 8 μm pore polycarbonate membranes (Corning). Briefly, 5×10^4 cells resuspended in serum-free DMEM were seeded into the upper chamber. The lower chamber contained DMEM supplemented with 10% FBS as a chemoattractant. After incubation for 24 hours at 37°C with 5% CO_2, non-migrated cells on the upper membrane surface were removed by cotton swab. Migrated cells on the lower membrane surface were fixed with 4% paraformaldehyde for 20 minutes, permeabilized, and stained with 0.1% crystal violet for 30 minutes. Membranes were rinsed in PBS, air-dried, and mounted on slides. Cell quantification was performed using bright-field microscopy (Leica) by capturing five random fields per membrane. Migrated cells were counted automatically using ImageJ software.

Flow Cytometry Immunophenotyping

Immune cells were isolated from tumor tissue using the Percoll density gradient centrifugation method and prepared as single-cell suspensions. All samples were stained with viability dye (423110, BioLegend) after pre-blocking with an Fc receptor blocking antibody (70–0161, Tonbo Biosciences). Subsequently, the cells were surface-stained with fluorescently labeled anti-CD45 (103130, BioLegend), anti-CD8 (563786, BioLegend), and anti-NK1.1 (108708, BioLegend) for phenotyping. Then the flow cytometry data analysis was performed using FlowJo software.

Apoptosis Assay

Cells were collected using EDTA-free trypsin, centrifuged at 1,800 rpm, 4°C for 5 min, and the supernatant discarded. The pellet was washed twice with ice-cold PBS, centrifuging under the same conditions each time. Cells were resuspended in 100 μL of 1× Binding Buffer. Next, 5 μL of Annexin V-FITC and 5 μL of PI Staining Solution (A211-01, Vazyme) were added and gently mixed. After incubating protected from light at room temperature for 10 min, 400 μL of 1× Binding Buffer was added and gently mixed. The stained samples were then analyzed by flow cytometry.

Lipid Peroxidation Assay

Cells were collected and centrifuged at 600g for 5 min at room temperature. After discarding the supernatant, the pellet was resuspended in an appropriate volume of BODIPY™ 581/591 C11 (D3861, Invitrogen) working solution and incubated at 37°C for 20 min. Discarded the supernatant, cells were resuspended in a suitable volume of PBS and analyzed by flow cytometry.

Animal Studies

To assess YIF1B's tumorigenic role, 6-week-old male C57BL/6 and BALB/c nude mice complied with the Committee on the Ethics of Animal Experiments of Capital Medical University and received subcutaneous injections of 1×10^6 stable YIF1B-knockdown or control cells. Tumors were harvested after 4 weeks for dimensional and histopathological analysis.

Statistical Analysis

Statistical analyses were conducted using R v4.3.1 and GraphPad Prism v8.0. Continuous data are expressed as mean±SD. Non-normally distributed data were analyzed with Mann–Whitney *U*-tests, while parametric comparisons employed: independent t-tests (two groups) and ANOVA (≥3 groups). Spearman correlation assessed variable associations, and p-values from correlation analyses were adjusted for multiple comparisons using the Benjamini-Hochberg false discovery rate (FDR) method. Significance levels: *p<0.05, **p<0.01, ***p<0.001, ****p<0.0001.

Results

Identification of PANoptosis-Related Genes in HCC from Single-Cell Transcriptomics and TCGA Database

To identify key cellular clusters and pathogenic genes related to PANoptosis in HCC, we performed an in-depth analysis of the single-cell sequencing dataset, GSE202642. Using the KNN clustering algorithm, all cells were grouped into 11 distinct clusters (Figure 1A), with subsequent cell type annotation through marker gene expression visualization and UMAP dimensionality reduction to resolve six definitive populations: T cells (CD8A+), B cells (CD79A+), NK cells, myeloid cells (FLT1+), endothelial cells (CD34+), fibroblasts (PDGFRB+), and epithelial cells (Figure 1B and C). Subsequently, the "PercentageFeatureSet" algorithm enabled cell-level PANoptosis quantification, with median expression thresholds stratifying cells into low or high PANoptosis subgroups.

The single-sample gene set enrichment analysis (ssGSEA) via the GSVA R package quantified PANoptosis-related gene enrichment in TCGA-HCC samples. Weighted gene co-expression network analysis (WGCNA) was identified PANoptosis-associated co-expression modules in the TCGA-HCC cohort. WGCNA delineated six color-coded modules (MEblue/brown/turquoise/yellow/green/red) under stringent parameters (soft-threshold=9, min-module-size=4, deepSplit=4, merge-threshold =0.25) (Figure S1A and S1B, Figure 1D and E).[21] The MEblue module, which exhibited the strongest negative correlation with PANoptosis score, was selected for further investigation. To identify candidate PANoptosis-related genes, we conducted machine-learning-based screening using genes from the MEblue module. The Least Absolute Shrinkage and Selection Operator (LASSO), Support Vector Machine (SVM), Extreme Gradient Boosting (XGBoost), and Gradient Boosting Machine (GBM) were used to identify the most diagnostically significant PANoptosis-related genes (Figure S2A–D). Four PANoptosis signature (CYBC1, JPT1, UQCRH, YIF1B) independently predicted survival in the TCGA cohort (Figure 1F and G).[22]

Validation of a PANoptosis-Related Prognostic Model in HCC

The PANoptosis-derived prognostic signature was calculated as a weighted sum of the four identified gene expression values (Figure 2A). The model demonstrated strong predictive power in TCGA cohort, with time-dependent AUCs of 0.691 (1-year), 0.650 (3-year), and 0.661 (5-year) (Figure 2B). Median-stratified risk scoring revealed significantly poorer OS in high-risk patients (Figure 2C). External validation (GSE16747) yielded 1/3/5-year RFS AUCs of 0.678/0.699/0.761, confirming prognostic robustness (Figure 2D).[23] Consistent with the training set, high-risk HCC patients exhibited poorer overall survival and recurrence-free survival compared to low-risk patients (Figure 2E and F). All four genes were consistently upregulated in high-risk patients, underscoring their clinical utility as PANoptosis-associated prognostic biomarkers of HCC.

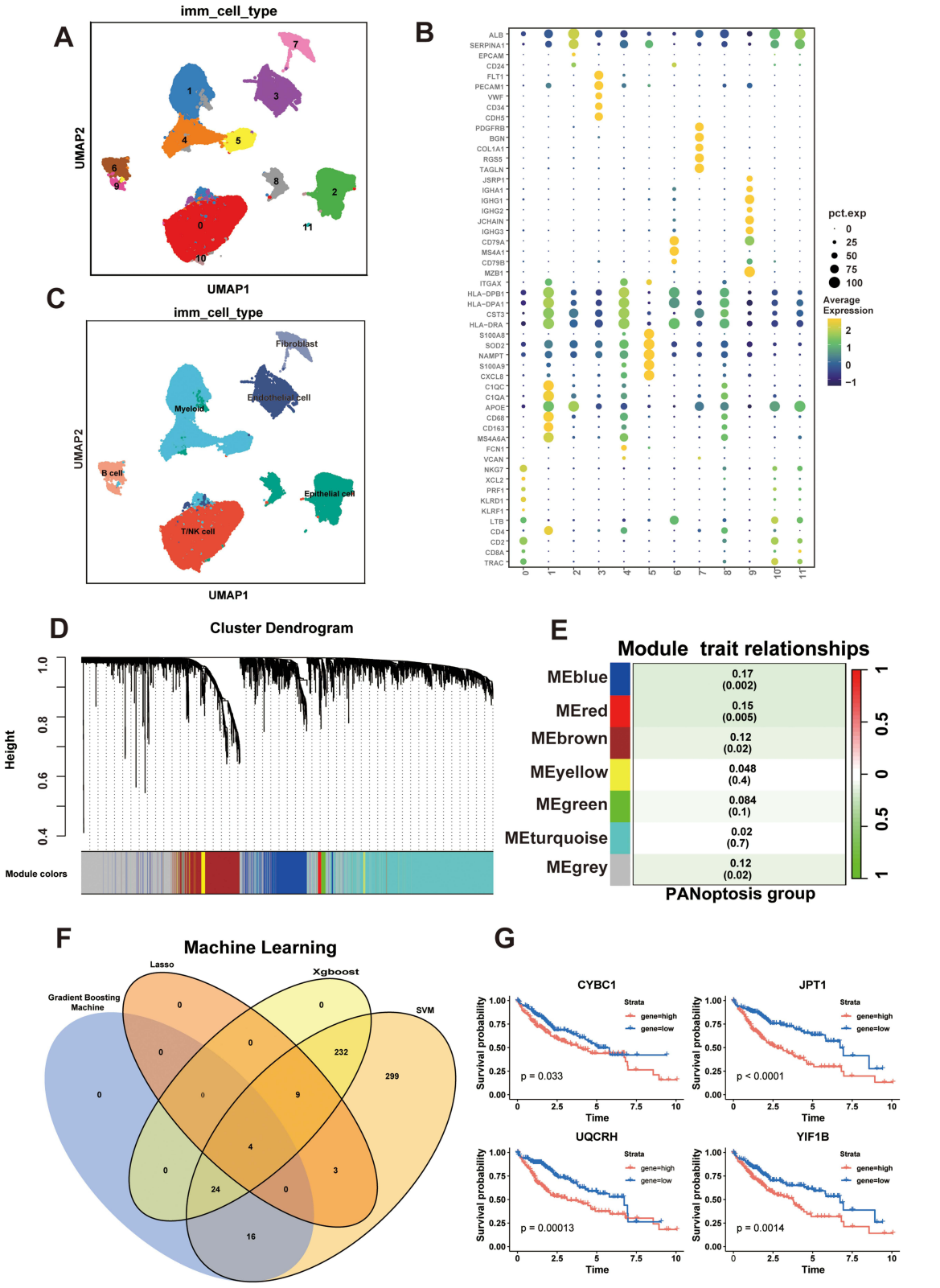

Figure 1 Identification of PANoptosis-Related Genes in HCC from Single-Cell Transcriptomics and TCGA Database. (**A**) Umap visualization for clustering. (**B** and **C**) Different cell types identified by the expression of surface marker genes. (**D** and **E**) WGCNA identifies MEtan module as the most strongly correlated with PANoptosis activity. (**F**) LASSO, SVM, XGBoost and GBM to identify the most diagnostically significant PANoptosis-related genes. (**G**) Four PANoptosis-related genes associated with survival outcomes in the TCGA cohort.

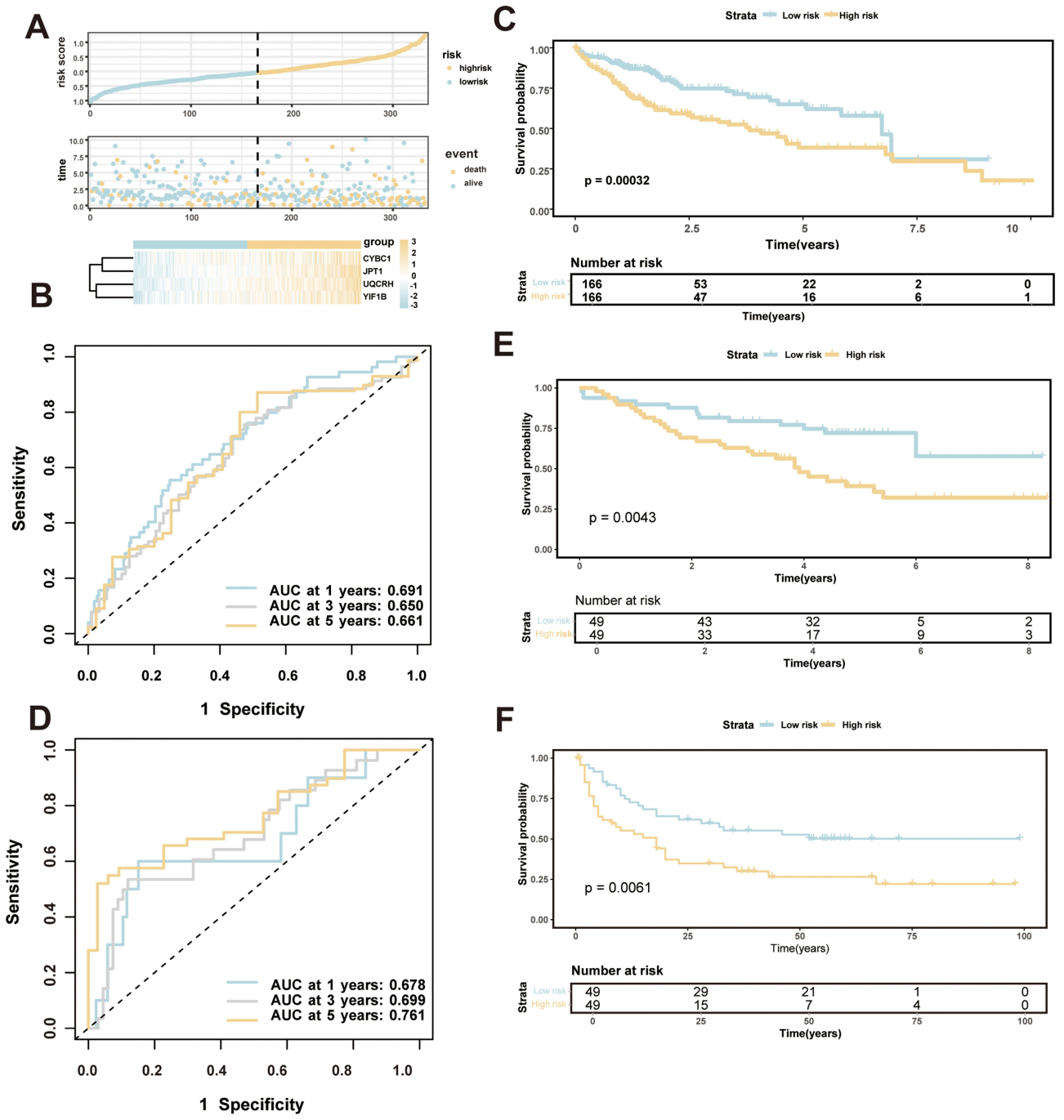

Figure 2 Validation of a PANoptosis-Related Prognostic Model in HCC. (**A**) Risk stratification visualization: distribution of risk scores, survival status, and signature gene expression patterns in the training cohort. (**B**) Time-dependent ROC curves validate predictive accuracy in TCGA cohorts. (**C**) Kaplan-Meier analysis reveals significantly poorer overall survival in high-risk TCGA-HCC patients. (**D**) Time-dependent ROC curves validate predictive accuracy in GSE16747 cohort. (**E** and **F**) High-risk HCC patients exhibited poorer overall survival and recurrence-free survival in GSE16747 cohort.

High-Risk Groups Demonstrate Impaired Antitumor Immune Response

We investigated the relationship between PANoptosis model scores and immune infiltration in HCC. Single-sample GSEA (ssGSEA) of 28 immune cell subtypes revealed reduced infiltration of NK cells, memory B cells, and Th1 cells in high-risk groups, along with elevated MDSCs, activated CD4+T cells, and macrophages (Figure 3A).[24] Similarly, PANoptosis-associated genes (CYBC1, JPT1, UQCRH, and YIF1B) were positively correlated with pro-tumor immune subsets (MDSCs, activated CD4+T cells, and macrophages) (Figure 3B), suggesting immunosuppressive microenvironments in high-risk groups.

https://doi.org/10.2147/JHC.S533777

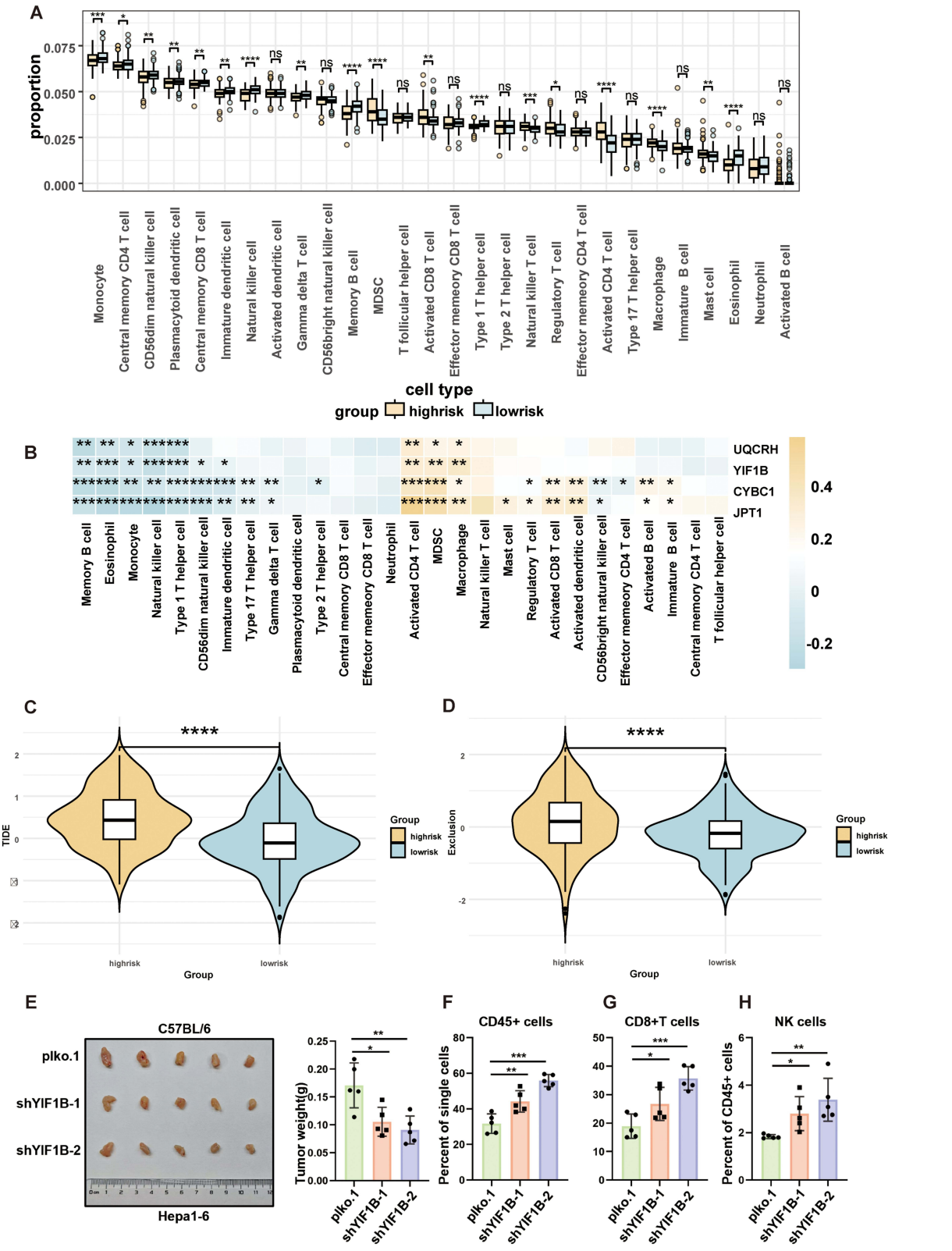

Figure 3 High-Risk Groups Demonstrate Impaired Antitumor Immune Response. (**A**) 28 immune cell subtypes expressed differences between high-risk and low-risk groups evaluated by ssGSEA. (**B**) The correlation of PANoptosis-associated genes (CYBC1, JPT1, UQCRH and YIF1B) with 28 immune cell subtypes. (**C** and **D**) The difference of TIDE scores, Dysfunction, Exclusion, MSI and MDSC in high-risk and low-risk groups. (**E**) Hepa1-6 cells stably transfected with empty vector or shYIF1B were subcutaneously injected into C57BL/6. Tumor weight was quantitatively analyzed after 3 weeks. (**F–H**) Tumor-infiltrating immune cells were detected by flow cytometry in empty vector or shYIF1B tumors.

Note: *p<0.05, **p<0.01, ***p<0.001, ****p<0.0001.

We further evaluated tumor immune dysfunction and exclusion (TIDE) scores, established predictors of immunotherapy response.[25] Enhanced immunotherapy responses were predicted by lower TIDE scores (Figure S3A). The low-risk group exhibited lower TIDE scores and reduced MDSC infiltration (Figure 3C and D, Figure S3B and S3C), indicating diminished immune evasion and an enhanced immunotherapy response. To investigate the impact of YIF1B on the tumor immune microenvironment, we established a stable YIF1B-knockdown Hepa1-6 cell line and subcutaneously injected these cells into C57BL/6 mice. Tumor harvest and weighing at three weeks post-injection revealed that YIF1B knockdown significantly inhibited the in vivo tumorigenic capacity of hepatocellular carcinoma cells (Figure 3E). Flow cytometric analysis of tumor tissues demonstrated that YIF1B deficiency markedly increased the proportion of tumor-infiltrating immune cells, notably CD8+T cell and NK cell subsets (Figure 3F–H). These observed correlation with diminished immune checkpoint gene expression in low-risk patients suggests enhanced immunotherapy responsiveness.

High-Risk Groups Exhibit Elevated Tumor Mutation Burden

To investigate the PANoptosis-associated tumor mutation burden (TMB), we analyzed the mutation count and spectrum of PANoptosis-related genes.[26] Elevated PANoptosis risk scores positively correlated with TMB in high-risk cohorts (Figure 4A). Interestingly, male patients exhibited significantly higher mutation counts than females across the entire cohort (Figure 4B).

Comparative Maftools analysis of prioritized somatic variants (top 30) demonstrated significantly elevated mutational burden in TCGA high-risk cohorts compared to low-risk counterparts (Figure 4C and D).[27] TP53 exhibited the highest mutational prevalence in high-risk cohorts, demonstrating a 25% elevated frequency compared to low-risk counterparts. Notably, most TP53 mutations are missense variants, likely impairing tumor-suppressive function and promoting cell cycle dysregulation, which may drive aggressive phenotypes in high-risk HCC.

High-Risk Groups Exhibit Poor Response to Sorafenib and Chemotherapies

While sorafenib demonstrates survival benefits in unresectable HCC, its therapeutic efficacy remains constrained by acquired resistance mechanisms.[28,29] Analysis of two independent sorafenib-treated HCC cohorts revealed elevated PANoptosis risk scores in non-responders, suggesting resistance in high-risk groups (Figure 5A).

To evaluate chemotherapy sensitivity, we calculated IC50 values for standard chemotherapeutic agents using the Cancer Genome Project (CGP) database.[30] The low-risk group demonstrated significantly lower IC50 values for multiple drugs, including Bortezomib_1191, Docetaxel_1007, Fulvestrant_1816, Temozolomide_1375, and Vinblastine_1818 (Figure 5B–F), indicating enhanced therapeutic susceptibility.[31,35] These findings underscore the clinical utility of PANoptosis risk stratification for guiding personalized HCC treatment.

PANoptosis Risk Scores as Prognostic Determinants and Validation of Nomograms

To assess the clinical relevance of PANoptosis risk scores in HCC patients, multivariable Cox analyses integrating PANoptosis risk scores with clinicopathological parameters (age, gender, tumor stage) identified elevated PANoptosis scores and advanced tumor stage as independent predictors of reduced overall survival (Figure 6A and B). The PANoptosis score emerges as a validated independent predictor for HCC prognosis.

To enhance clinical utility, a risk-stratification nomogram incorporating PANoptosis scores demonstrated robust predictive accuracy, which was assessed using calibration curves and the C-index (Figure 6C and D). Decision curve analysis demonstrated enhanced clinical utility over established parameters (Figure 6E), while time-dependent ROC curves validated consistent prognostic accuracy across 1/3/5-year intervals (AUC=0.711, 0.705, and 0.712) (Figure 6F–H). Risk stratification by median scores delineated significant survival disparities, with high-risk groups exhibiting markedly shorter survival times (Figure 6I).

YIF1B Promotes the Growth and Tumorigenesis of HCC

YIF1B (Yip1 Interacting Factor Homolog B), a Golgi-ER membrane trafficking modulator, exhibits pan-cancer oncogenicity.[36] It belongs to the Yip1 domain protein family, which is mainly associated with membrane transport between the endoplasmic reticulum (ER) and the Golgi apparatus.[37] YIF1B dysregulation has been documented across multiple malignancies including breast and lung cancers, implicating its potential role in neoplastic progression. However, the mechanism and its role in HCC pathogenesis remains unclear.[38]

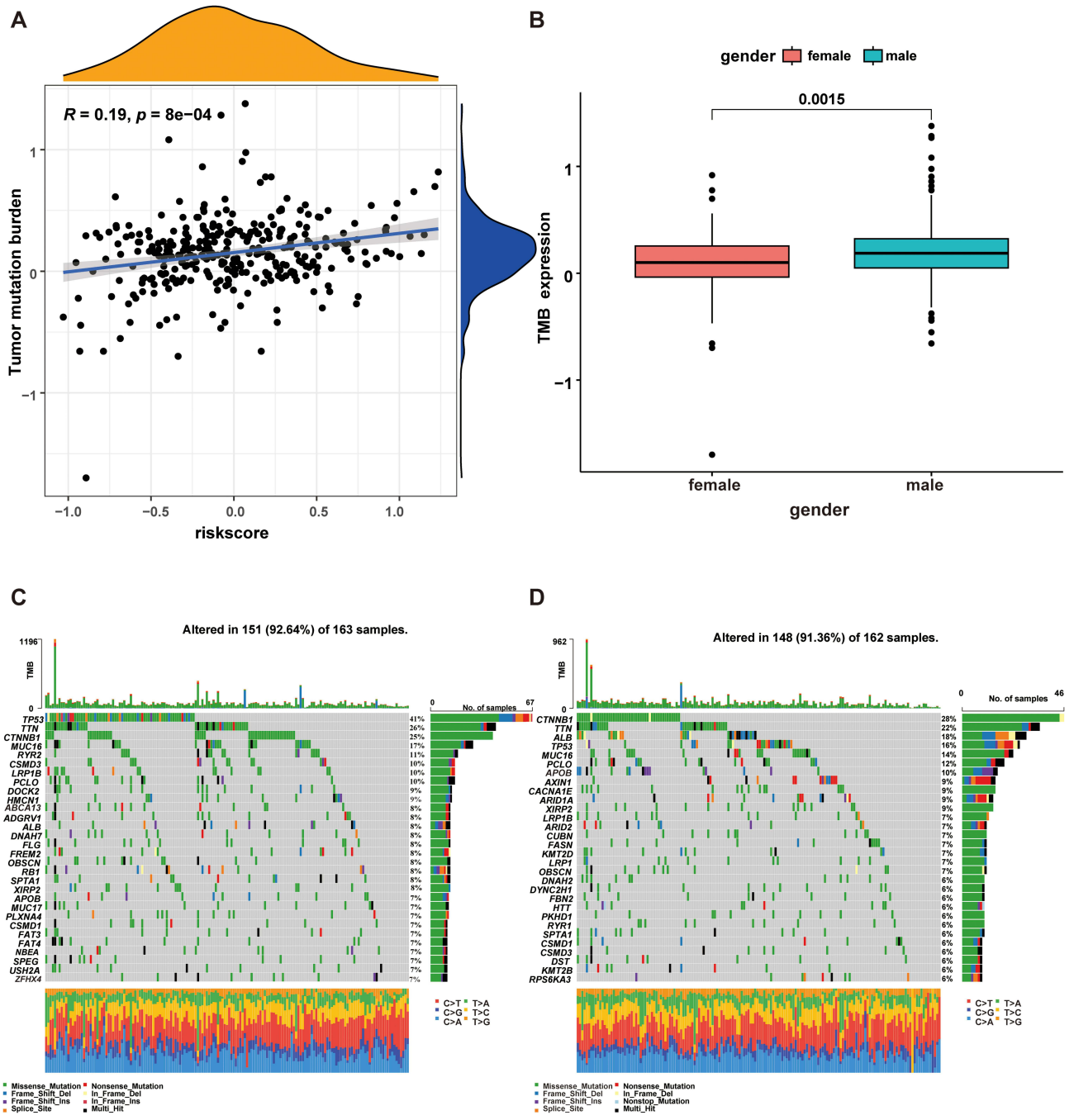

Figure 4 High-Risk Groups Exhibit Elevated Tumor Mutation Burden. (**A**) The correlation of risk score with TMB. (**B**) The difference TMB between male and female. (**C** and **D**) The high-risk group exhibited a higher mutation frequency overall.

To investigate the functional role of YIF1B in HCC progression, we employed lentiviral-mediated gene manipulation in HepG2 and Huh7 cell lines. Cells were transduced to stably overexpress or knockdown YIF1B. We observed that YIF1B knockdown promoted apoptosis in HepG2 cells and induced lipid peroxidation accumulation in Huh7 cells. These results indicate that YIF1B depletion accelerates tumor cell death by concurrently activating both apoptotic and ferroptotic pathways in HCC cells (Figure S4A and B). This finding further supports the central role of YIF1B as a PANoptosis regulator in cellular demise pathways. Subsequent CCK-8 proliferation assays revealed that YIF1B overexpression significantly enhanced cellular growth in HCC cell lines. Conversely, YIF1B knockdown markedly suppressed proliferation compared to control groups (Figure 7A and B).

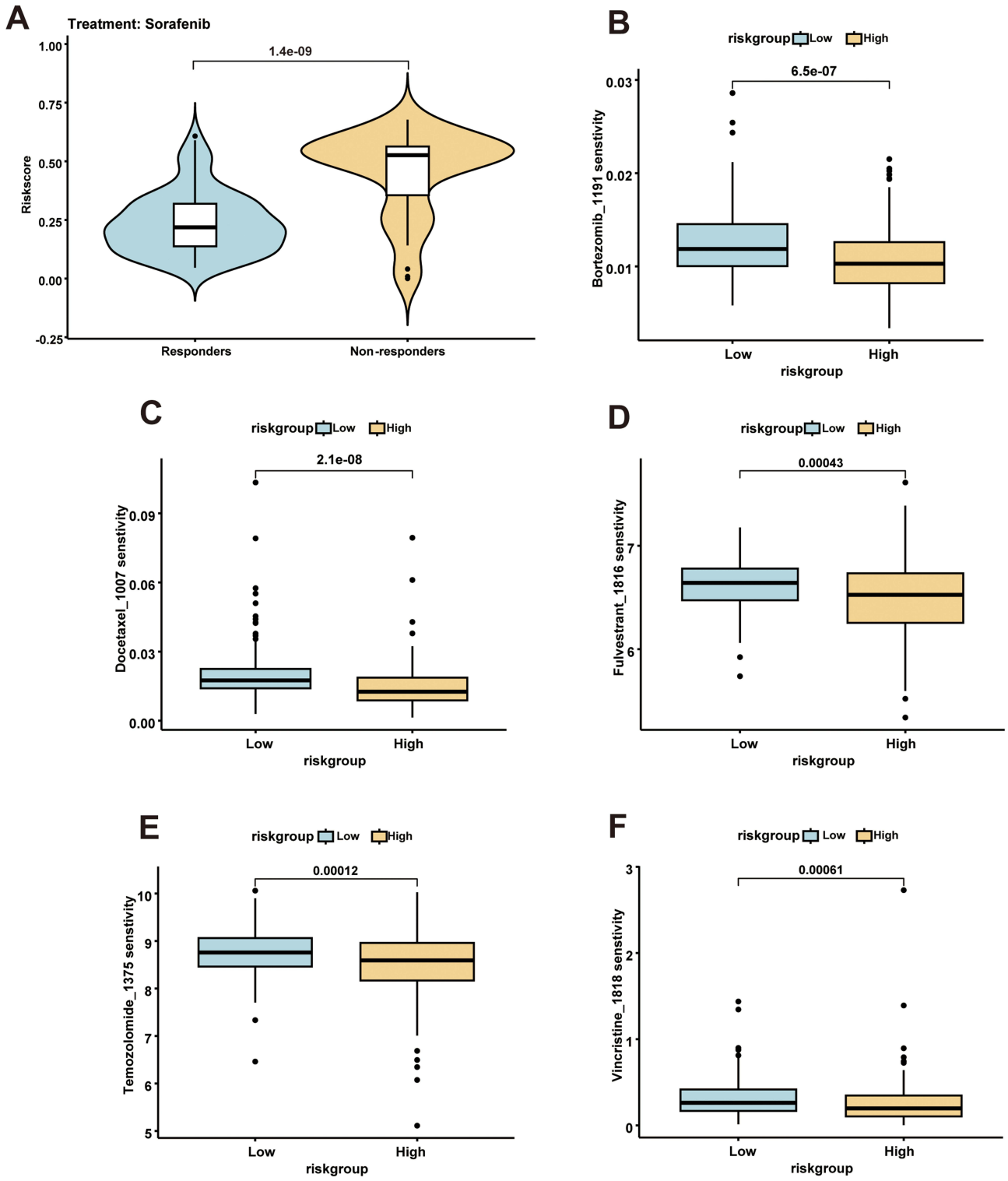

Figure 5 High-Risk Groups Exhibit Poor Response to Sorafenib and Chemotherapies. (**A**) The correlation of risk score with sorafenib. (**B**–**F**) The low-risk group had lower IC50 values for Bortezomib_1191, Docetaxel_1007, Fulvestrant_1816, Temozolomide_1375 and Vinblastine_1818.

To further assess metastatic potential, transwell migration assays were performed. Consistent with the proliferation data, YIF1B-overexpressing cells exhibited a pronounced increase in migratory capacity. In stark contrast, YIF1B knockdown strongly inhibited cell migration (Figure 7C). Collectively, these in vitro results demonstrate that YIF1B critically regulates both proliferative and metastatic phenotypes in HCC cells.

https://doi.org/10.2147/JHC.S533777

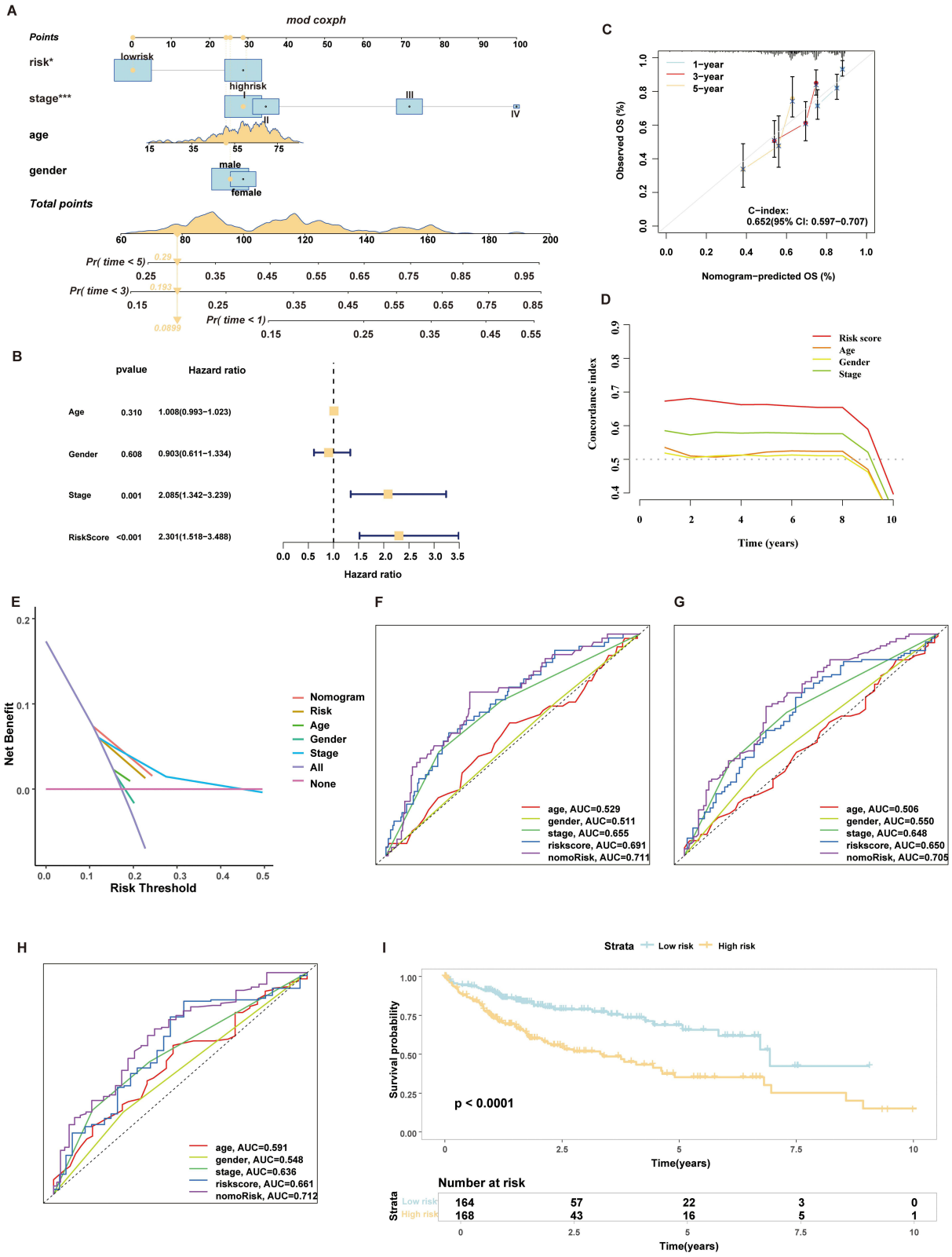

Figure 6 PANoptosis Risk Scores as Prognostic Determinants and Validation of Nomograms. (**A** and **B**) A nomogram was developed via integrating clinical data and PANoptosis scores. (**C** and **E**) The calibration curves, the C-index and DCA were assessed the accuracy of the nomogram. (**F**–**H**) The predictive ability of the nomogram confirmed by multivariable ROC curve analysis. (**I**) The stability of nomogram was validated by survival curves.

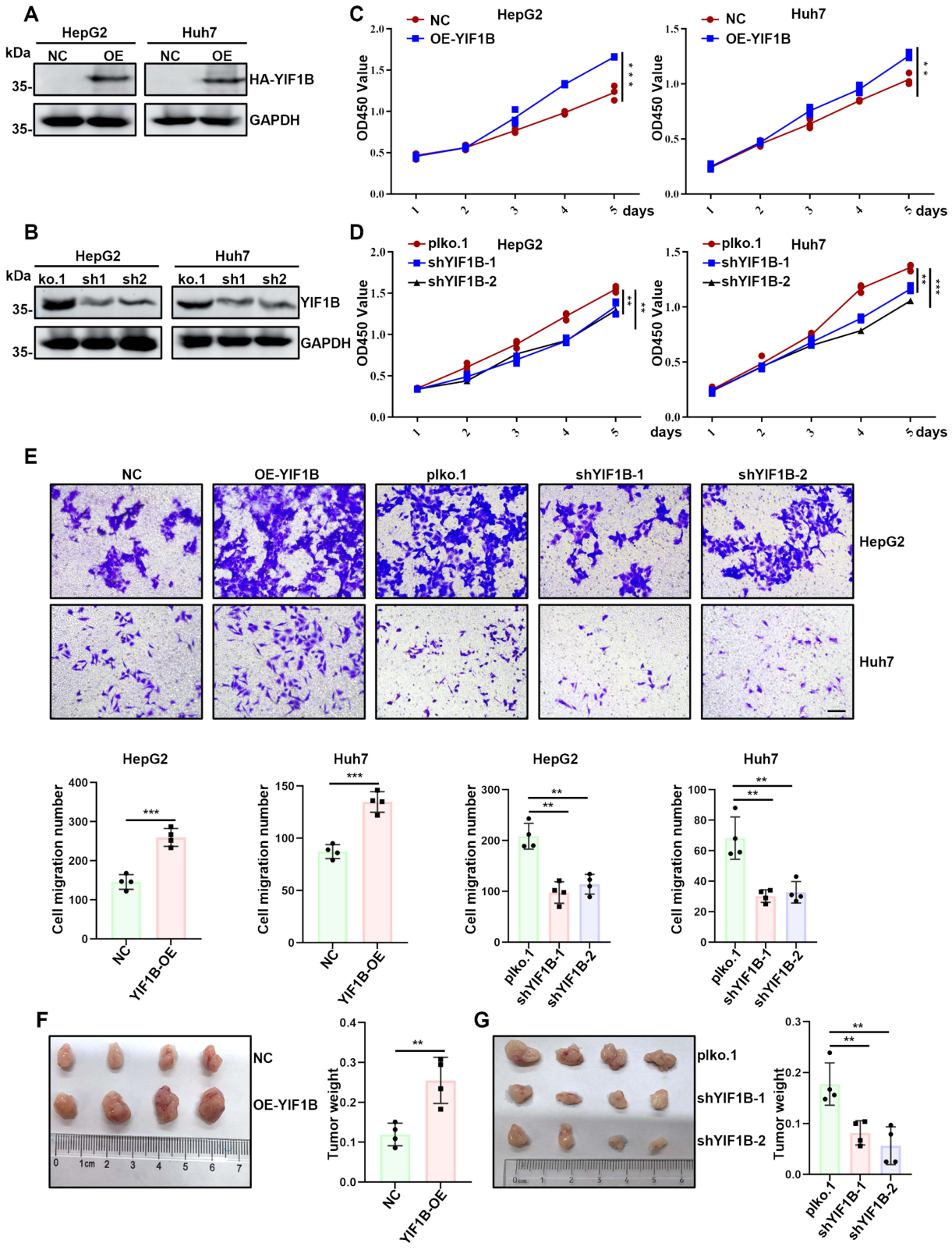

Figure 7 YIF1B Promotes the Growth and Tumorigenesis of HCC. (**A** and **B**) The protein levels of YIF1B and GAPDH were detected by Western blotting in HepG2 and Huh7 cells transfected with HA-YIF1B or with shYIF1B. (**C** and **D**) Proliferation rates of the cells above were measured by CCK-8 assays. (**E**) The migratory potential of HepG2 and Huh7 cells transfected with HA-YIF1B or with shYIF1B were measured by transwell assay. Scale bar, 200μm. (**F** and **G**) HepG2 cells stably transfected with empty vector, HA-YIF1B or shYIF1B were subcutaneously injected into nude mice. Tumor weight was quantitatively analyzed after 4 weeks.
Note: Date was the mean±SD. **p<0.01, ***p<0.001.

https://doi.org/10.2147/JHC.S533777

We next evaluated the oncogenic role of YIF1B in vivo using a xenograft tumor model. HepG2 cells stably expressing empty vector, overexpress or knockdown YIF1B were subcutaneously injected into 6-week-old BALB/c nude mice. Tumor growth was monitored longitudinally. Mice implanted with YIF1B overexpression cells developed significantly larger and faster-growing tumors than the control group. Remarkably, tumors derived from knockdown YIF1B cells showed profound growth suppression, with substantially reduced tumor volume and weight compared to controls (Figure 7D and E). Overall, our results suggest that YIF1B plays a critical regulatory role in the growth and tumorigenesis of HCC. Targeting YIF1B may become a potential new strategy for the treatment of HCC.IF1B as a master regulator of HCC pathogenesis, highlighting its therapeutic vulnerability.

Discussion

By leveraging single-cell transcriptomic datasets from HCC, this study employed advanced bioinformatics pipelines to systematically investigate the clinical and mechanistic relevance of the PANoptosis-related genes. Rigorous machine-learning algorithms identified four pivotal PANoptosis-related hub genes (CYBC1, JPT1, UQCRH, and YIF1B), stratifying patients with HCC into distinct prognostic clusters. The high-risk group exhibited significantly reduced overall and relapse-free survival, accompanied by immunosuppressive features and an elevated tumor mutational burden. Pharmacogenomic analyses have demonstrated differential therapeutic vulnerabilities, with high-risk groups showing resistance to sorafenib and low-risk groups displaying enhanced responsiveness to conventional chemotherapeutic agents.

Mechanistically, YIF1B, a Golgi apparatus-associated trafficking regulator, exerts oncogenic effects through the dysregulation of Golgi-mediated protein sorting and vesicular trafficking, thereby compromising cellular homeostasis.[39] Although previous pan-cancer studies have documented YIF1B overexpression, its direct mechanism of involvement in HCC pathogenesis remains unclear. Our multi-dimensional functional validation revealed that YIF1B is a PANoptosis-associated oncogene, and that YIF1B knockout attenuates malignant progression, whereas its overexpression potentiates oncogenic phenotypes in vitro and in vivo. These findings suggest that YIF1B is a master regulator of HCC cellular dynamics, orchestrating proliferation equilibrium through PANoptosis modulation.

This study establishes PANoptosis-related gene signatures as robust prognostic biomarkers, while nominating YIF1B as a druggable target for precision HCC therapeutics. The observed correlation between the PANoptosis risk strata and chemotherapeutic sensitivity underscores the clinical utility of this framework for treatment stratification. Current limitations, including incomplete characterization of the YIF1B interactome and tumor microenvironment crosstalk, present opportunities for future investigation. Prioritizing the development of YIF1B specific inhibitors and elucidating their downstream effectors hold significant promise for advancing precision oncology paradigms in HCC management.

Conclusion

This study identified four PANoptosis-related genes (CYBC1, JPT1, UQCRH, and YIF1B) through integrative analysis of HCC single-cell transcriptomic data. Elevated PANoptosis signatures are associated with poor survival outcomes, immunosuppressive microenvironment, and resistance to sorafenib treatment. The PANoptosis-based risk stratification correlates with chemosensitivity, underscoring its clinical promise. Most significantly, therapeutic targeting of YIF1B and its interactome emerges as a translatable approach to expand precision treatment options for HCC patients.

Abbreviations

HCC, hepatocellular carcinoma; YIF1B, Yip1 Interacting Factor Homolog B; TCGA, The Cancer Genome Atlas; GSEA, gene set enrichment analysis; WGCNA, weighted gene co-expression network analysis; TIDE, tumor immune dysfunction and exclusion scores; TMB, tumor mutation burden; MSI, microsatellite instability; TME, tumor microenvironment; CGP, Cancer Genome Project.

Data Sharing Statement

This study did not generate new unique reagents. The plasmids and cell lines are available upon request. Further information and requests for resources should be directed and fulfilled by the xiwang@ccmu.edu.cn. All data generated or analyzed during this study are available from the corresponding author upon reasonable request.

Ethics Statement

This study was approved by the Animal Experiment Ethics Committee of Capital Medical University (No. AEEI-2024-291, Beijing, China) and strictly adhered to the animal welfare requirements specified in the China national standards "Laboratory Animals - Guidelines for Welfare Ethical Review" (GB/T 35892-2018) and "Guidelines for Laboratory Animal Welfare and Occupational Health Safety Inspection" (RB/T 018-2019). All data analyzed in this study were sourced from the publicly available TCGA database, which adheres to the NIH Genomic Data Sharing Policy with fully de-identified datasets containing no directly or indirectly identifiable private information. This study complies with the TCGA Data Use Certification Agreement (DUCA) for non-commercial research purposes. Secondary analysis of public data aligns with the ethical principles of the Declaration of Helsinki. Ethics Approval (KY2024-008-01), approved by Beijing Ditan Hospital.

Author Contributions

All authors made a significant contribution to the work reported, whether in the conception, study design, execution, acquisition of data, analysis, and interpretation, or in all these areas, took part in drafting, revising, or critically reviewing the article; gave final approval of the version to be published; have agreed on the journal to which the article has been submitted; and agree to be accountable for all aspects of the work.

Funding

This work was financially supported by the National Natural Science Foundation of China (32270635), Natural Science Foundation of Beijing (7232082,5254029), and Science Foundation of Beijing Ditan Hospital, Capital Medical University (DTOL-202405).

Disclosure

The authors declare no competing interests for this work.

References

1. Yeo YH, Abdelmalek M, Khan S, et al. Current and emerging strategies for the prevention of hepatocellular carcinoma. *Nat Rev Gastroenterol Hepatol*. 2025;22(3):173–190. doi:10.1038/s41575-024-01021-z
2. Llovet JM, De Baere T, Kulik L, et al. Locoregional therapies in the era of molecular and immune treatments for hepatocellular carcinoma. *Nat Rev Gastroenterol Hepatol*. 2021;18(5):293–313. doi:10.1038/s41575-020-00395-0
3. Vogel A, Meyer T, Sapisochin G, Salem R, Saborowski A. Hepatocellular carcinoma. *Lancet*. 2022;400(10360):1345–1362. doi:10.1016/S0140-6736(22)01200-4
4. Yang C, Zhang H, Zhang L, et al. Evolving therapeutic landscape of advanced hepatocellular carcinoma. *Nat Rev Gastroenterol Hepatol*. 2023;20(4):203–222. doi:10.1038/s41575-022-00704-9
5. Chan YT, Zhang C, Wu J, et al. Biomarkers for diagnosis and therapeutic options in hepatocellular carcinoma. *Mol Cancer*. 2024;23(1):189. doi:10.1186/s12943-024-02101-z
6. Oura K, Morishita A, Tani J, Masaki T. Tumor immune microenvironment and immunosuppressive therapy in hepatocellular carcinoma: a review. *Int J Mol Sci*. 2021;22(11):5801. doi:10.3390/ijms22115801
7. Sun C, Mezzadra R, Schumacher TN. Regulation and function of the PD-L1 checkpoint. *Immunity*. 2018;48(3):434–452. doi:10.1016/j.immuni.2018.03.014
8. Agarwal S, Aznar MA, Rech AJ, et al. Deletion of the inhibitory co-receptor CTLA-4 enhances and invigorates chimeric antigen receptor T cells. *Immunity*. 2023;56(10):2388–2407.e2389. doi:10.1016/j.immuni.2023.09.001
9. Jia WT, Xiang S, Zhang JB, et al. Jiedu recipe, a compound Chinese herbal medicine, suppresses hepatocellular carcinoma metastasis by inhibiting the release of tumor-derived exosomes in a hypoxic microenvironment. *J Integr Med*. 2024;22(6):696–708. doi:10.1016/j.joim.2024.10.002
10. Wang J, Lu Y, Zhang R, et al. Modulating and imaging macrophage reprogramming for cancer immunotherapy. *Phenomics*. 2024;4(4):401–414. doi:10.1007/s43657-023-00154-6
11. Wang J, Chen Y, Xu Y, et al. DNASE1L3-mediated PANoptosis enhances the efficacy of combination therapy for advanced hepatocellular carcinoma. *Theranostics*. 2024;14(17):6798–6817. doi:10.7150/thno.102995
12. Kesavardhana S, Malireddi RKS, Kanneganti TD. Caspases in cell death, inflammation, and pyroptosis. *Annu Rev Immunol*. 2020;38:567–595. doi:10.1146/annurev-immunol-073119-095439
13. Galluzzi L, Vitale I, Aaronson SA, et al. Molecular mechanisms of cell death: recommendations of the nomenclature committee on cell death 2018. *Cell Death Differ*. 2018;25(3):486–541. doi:10.1038/s41418-017-0012-4
14. Wei W, Wang H, Ren C, et al. Ultrasmall enzyodynamic panoptosis nano-inducers for ultrasound-amplified hepatocellular carcinoma therapy and lung metastasis inhibition. *Adv Mater*. 2024;36(45):e2409618. doi:10.1002/adma.202409618
15. Zhou L, Lyu J, Liu F, Su Y, Feng L, Zhang X. Immunogenic PANoptosis-initiated cancer sono-immune reediting nanotherapy by iteratively boosting cancer immunity cycle. *Adv Mater*. 2024;36(2):e2305361. doi:10.1002/adma.202305361

16. You YP, Yan L, Ke HY, et al. Baicalin inhibits PANoptosis by blocking mitochondrial Z-DNA formation and ZBP1-PANoptosome assembly in macrophages. *Acta Pharmacol Sin*. 2025;46(2):430–447. doi:10.1038/s41401-024-01376-8
17. Pandeya A, Kanneganti TD. Therapeutic potential of PANoptosis: innate sensors, inflammasomes, and RIPKs in PANoptosomes. *Trends Mol Med*. 2024;30(1):74–88. doi:10.1016/j.molmed.2023.10.001
18. Shen J, San W, Zheng Y, et al. Different types of cell death in diabetic endothelial dysfunction. *Biomed Pharmacother*. 2023;168:115802. doi:10.1016/j.biopha.2023.115802
19. Gao L, Shay C, Teng Y. Cell death shapes cancer immunity: spotlighting PANoptosis. *J Exp Clin Cancer Res*. 2024;43(1):168. doi:10.1186/s13046-024-03089-6
20. Hou G, Chen Y, Lei H, Lu S, Cheng L. Nanomaterials-induced panoptosis: a promising anti-tumor strategy. *Angew Chem Int Ed Engl*. 2025;64(5):e202419649. doi:10.1002/anie.202419649
21. Luo Y, Coskun V, Liang A, et al. Single-cell transcriptome analyses reveal signals to activate dormant neural stem cells. *Cell*. 2015;161(5):1175–1186. doi:10.1016/j.cell.2015.04.001
22. Tang G, Qi L, Sun Z, et al. Evaluation and analysis of incidence and risk factors of lower extremity venous thrombosis after urologic surgeries: a prospective two-center cohort study using LASSO-logistic regression. *Int J Surg*. 2021;89:105948. doi:10.1016/j.ijsu.2021.105948
23. Liu YS, Yang CY, Chiu PF, et al. Machine learning analysis of time-dependent features for predicting adverse events during hemodialysis therapy: model development and validation study. *J Med Internet Res*. 2021;23(9):e27098. doi:10.2196/27098
24. Peng Z, Ye M, Ding H, Feng Z, Hu K. Spatial transcriptomics atlas reveals the crosstalk between cancer-associated fibroblasts and tumor microenvironment components in colorectal cancer. *J Transl Med*. 2022;20(1):302. doi:10.1186/s12967-022-03510-8
25. Zhang L, Zhang X, Liu H, et al. MTFR2-dependent mitochondrial fission promotes HCC progression. *J Transl Med*. 2024;22(1):73. doi:10.1186/s12967-023-04845-6
26. Chalmers ZR, Connelly CF, Fabrizio D, et al. Analysis of 100,000 human cancer genomes reveals the landscape of tumor mutational burden. *Genome Med*. 2017;9(1):34. doi:10.1186/s13073-017-0424-2
27. Sherman MA, Yaari AU, Priebe O, Dietlein F, Loh PR, Berger B. Genome-wide mapping of somatic mutation rates uncovers drivers of cancer. *Nat Biotechnol*. 2022;40(11):1634–1643. doi:10.1038/s41587-022-01353-8
28. Tang W, Chen Z, Zhang W, et al. The mechanisms of sorafenib resistance in hepatocellular carcinoma: theoretical basis and therapeutic aspects. *Signal Transduct Target Ther*. 2020;5(1):87. doi:10.1038/s41392-020-0187-x
29. Qin S, Kudo M, Meyer T, et al. Tislelizumab vs sorafenib as first-line treatment for unresectable hepatocellular carcinoma: a phase 3 randomized clinical trial. *JAMA Oncol*. 2023;9(12):1651–1659. doi:10.1001/jamaoncol.2023.4003
30. Fukada I, Mori S, Hayashi N, et al. Prognostic impact of cancer genomic profile testing for advanced or metastatic solid tumors in clinical practice. *Cancer Sci*. 2023;114(12):4632–4642. doi:10.1111/cas.15993
31. Li L, Zhang Y, Zhou Y, et al. Quaternary nanoparticles enable sustained release of bortezomib for hepatocellular carcinoma. *Hepatology*. 2022;76(6):1660–1672. doi:10.1002/hep.32584
32. Xu Z, Chen L, Gu W, et al. The performance of docetaxel-loaded solid lipid nanoparticles targeted to hepatocellular carcinoma. *Biomaterials*. 2009;30(2):226–232. doi:10.1016/j.biomaterials.2008.09.014
33. Williams MM, Spoelstra NS, Arnesen S, et al. Steroid hormone receptor and infiltrating immune cell status reveals therapeutic vulnerabilities of ESR1-mutant breast cancer. *Cancer Res*. 2021;81(3):732–746. doi:10.1158/0008-5472.CAN-20-1200
34. Muñoz-Gámez JA, López Viota J, Barrientos A, et al. Synergistic cytotoxicity of the poly (ADP-ribose) polymerase inhibitor ABT-888 and temozolomide in dual-drug targeted magnetic nanoparticles. *Liver Int*. 2015;35(4):1430–1441. doi:10.1111/liv.12586
35. Zhao Y, Chen J, Wei W, Qi X, Li C, Ren J. The dual-inhibitory effect of miR-338-5p on the multidrug resistance and cell growth of hepatocellular carcinoma. *Signal Transduct Target Ther*. 2018;3:3. doi:10.1038/s41392-017-0003-4
36. Liu J, Chen Z, Zhao P, Li W. Prognostic and immune regulating roles of YIF1B in pan-cancer: a potential target for both survival and therapy response evaluation. *Biosci Rep*. 2020;40(7). doi:10.1042/BSR20201384
37. Diaz J, Gérard X, Emerit MB, et al. YIF1B mutations cause a post-natal neurodevelopmental syndrome associated with Golgi and primary cilium alterations. *Brain*. 2020;143(10):2911–2928. doi:10.1093/brain/awaa235
38. Graab P, Bock C, Weiss K, et al. Lysosomal targeting of the ABC transporter TAPL is determined by membrane-localized charged residues. *J Biol Chem*. 2019;294(18):7308–7323. doi:10.1074/jbc.RA118.007071
39. AlMuhaizea M, AlMass R, AlHargan A, et al. Truncating mutations in YIF1B cause a progressive encephalopathy with various degrees of mixed movement disorder, microcephaly, and epilepsy. *Acta Neuropathol*. 2020;139(4):791–794. doi:10.1007/s00401-020-02128-8